Biochimica et Biophysica Acta 1823 (2012) 1697–1707

Contents lists available at SciVerse ScienceDirect

Biochimica et Biophysica Acta

journal homepage: www.elsevier.com/locate/bbamcr

Real-time analysis of intracellular glucose and calcium in pancreatic beta cells by fluorescence microscopy

Martin Tobias Kaminski [a], Sigurd Lenzen [a], Simone Baltrusch [a,b,*]

[a] Institute of Clinical Biochemistry, Hannover Medical School, 30623 Hannover, Germany
[b] Institute of Medical Biochemistry and Molecular Biology, University of Rostock, 18057 Rostock, Germany

ARTICLE INFO

Article history:
Received 19 January 2012
Received in revised form 13 June 2012
Accepted 15 June 2012
Available online 23 June 2012

Keywords:
Glucokinase
GLUT2
FLII[12]Pglu-700μ-δ6
Glucose metabolism
Calcium imaging
Pancreatic beta cell

ABSTRACT

Glucose is the physiological stimulus for insulin secretion in pancreatic beta cells. The uptake and phosphorylation of glucose initiate and control downstream pathways, resulting in insulin secretion. However, the temporal coordination of these events in beta cells is not fully understood. The recent development of the FLII[12]Pglu-700μ-δ6 glucose nanosensor facilitates real-time analysis of intracellular glucose within a broad concentration range. Using this fluorescence-based technique, we show the shift in intracellular glucose concentration upon external supply and removal in primary mouse beta cells with high resolution. Glucose influx, efflux, and metabolism rates were calculated from the time-dependent plots. Comparison of insulin-producing cells with different expression levels of glucose transporters and phosphorylating enzymes showed that a high glucose influx rate correlated with GLUT2 expression, but was largely also sustainable by high GLUT1 expression. In contrast, in cells not expressing the glucose sensor enzyme glucokinase glucose metabolism was slow. We found no evidence of oscillations of the intracellular glucose concentration in beta cells. Concomitant real-time analysis of glucose and calcium dynamics using FLII[12]Pglu-700μ-δ6 and fura-2-acetoxymethyl-ester determined a glucose threshold of 4 mM for the $[Ca^{2+}]_i$ increase in beta cells. Indeed, a glucose concentration of 7 mM had to be reached to evoke large amplitude $[Ca^{2+}]_i$ oscillations. The K_{ATP} channel closing agent glibenclamide was not able to induce large amplitude $[Ca^{2+}]_i$ oscillations in the absence of glucose. Our findings suggest that glucose has to reach a threshold to evoke the $[Ca^{2+}]_i$ increase and subsequently initiate $[Ca^{2+}]_i$ oscillations in a K_{ATP} channel independent manner.

1. Introduction

Glucose-stimulated insulin secretion from pancreatic beta cells determines the blood glucose concentration. Upon facilitative uptake via the glucose transporter 2 (GLUT 2) [1–3], glucose is phosphorylated by glucokinase and subsequently metabolized, leading to an increase in the ATP/ADP ratio [4–7]. This increase mediates the closure of ATP-sensitive potassium (K_{ATP}) channels, followed by depolarization of the plasma membrane, causing voltage-gated calcium channels to open [8]. Ultimately, insulin is released by an increase in intracellular free calcium ($[Ca^{2+}]_i$) [8–11]. However, this triggering pathway requires additional amplification signals generated through metabolic and neuronal mechanisms [8,12]. Exploring the interplay of these pathways is a significant challenge and requires sophisticated methodologies [8].

A rapid expansion in fluorescence-based sensors has facilitated real-time analysis of ions and metabolites, such as calcium [13], cAMP [14,15], and ATP [16–18] in intact cells. Such measurements display changes in metabolites with much higher resolution than static analyses requiring cell disruption [15,19]. Thus, live cell fluorescence microscopy approaches substantially contribute to our knowledge of regulatory networks controlling stimulus-secretion coupling in beta cells [20,21].

Glucose uptake and metabolism have been quantified in beta cells and islets using enzymatic assays and radiolabeled glucose analogs [22–26]. Fluorescence labeled glucose has also been used successfully to study glucose uptake [27,28]. In the past few years, so-called glucose nanosensors became available for intracellular glucose imaging in mammalian cells [19,20,29,30]. These nanosensors are based on the intramolecular fluorescence resonance energy transfer (FRET) response of an enhanced cyan fluorescent protein (ECFP)/citrine pair fused to a glucose-specific bacterial periplasmic binding protein [19,20]. A conformational change induced by glucose binding results in a concentration-dependent shift of the emission intensity ratios [29,30].

Abbreviations: GK, glucokinase; ECFP, enhanced cyan fluorescent protein; FRET, fluorescence resonance energy transfer; HK, hexokinase; GLUT, glucose transporter; MH, mannoheptulose; 3-OMG, 3-O-methylglucose; FLIPglu, FLII[12]Pglu-700μ-δ6; $[Ca^{2+}]_i$, intracellular calcium; G-6-P, glucose-6-phosphate

* Corresponding author at: Institute of Medical Biochemistry and Molecular Biology, University of Rostock, D-18057 Rostock, Germany. Tel.: +49 381 494 5760; fax: +49 381 494 5752.
E-mail address: simone.baltrusch@med.uni-rostock.de (S. Baltrusch).

0167-4889/$ – see front matter © 2012 Elsevier B.V. All rights reserved.
doi:10.1016/j.bbamcr.2012.06.022

Another advance in this development is FLII^{12}Pglu-700μ-δ6, a glucose nanosensor with a broad detection range of millimolar glucose concentrations [31–33]. The aim of the present study was to investigate changes in the intracellular glucose concentration in beta cells in real-time using this new glucose nanosensor in combination with simultaneous $[Ca^{2+}]_i$ measurements.

2. Materials and methods

2.1. Cellular FLIPglu expression

MIN6 and COS cells were grown in DMEM supplemented with 25 mM glucose, 10% (vol/vol) FCS, penicillin, and streptomycin in a humidified atmosphere at 37 °C and 5% CO_2. RINm5F cells were grown in RPMI 1640 supplemented with 10 mM glucose, 10% (vol/vol) FCS, penicillin, and streptomycin in a humidified atmosphere at 37 °C and 5% CO_2. INS1E cells were grown in RPMI 1640 supplemented with 10 mM glucose, 10% (vol/vol) FCS, 50 μM/l 2-mercaptoethanol, penicillin, and streptomycin in a humidified atmosphere at 37 °C and 5% CO_2. The pcDNA 3.1 vector was used for expression of FLII^{12}Pglu-700μ-δ6 (FLIPglu) (Addgene plasmid 17866) [32]. COS, RINm5F, and INS1E cells were transiently transfected using jetPEI (Qbiogene, Montreal, Canada). Stable MIN6 clones (MIN6-FLIPglu) were selected through resistance against G418 (250 μg/ml). Pancreatic islets were isolated from 6 to 10-week-old female NMRI mice by collagenase digestion in bicarbonate-buffered Krebs–Ringer solution. Beta cells were obtained using calcium-free Krebs–Ringer solution and kept in RPMI-1640 medium supplemented with 5 mM glucose. Cells were transduced at a multiplicity of infection of 10 for 2 h with adenoviral FLIPglu stock solution. Recombinant FLIPglu adenovirus was generated using the Ad-Easy viral vector system provided by B. Vogelstein (Baltimore, MD) [34]. The FLIPglu coding cDNA was subcloned as a SalI–NotI fragment into the pShuttle-CMV vector, and the recombinant adenoviral plasmid was generated by homologous recombination with the pAdEasy-1 plasmid in *Escherichia coli* BJ5183 cells. Adenoviruses were produced in 293 cells and purified by CsCl gradient centrifugation.

2.2. Recombinant FLIPglu generation

The full coding sequence of FLIPglu [32] was subcloned in-frame into the BamHI and NotI sites of the pGEX-6P-1 expression vector and expressed in the dark in *E. coli* BL21 using the glutathione S-transferase (GST) Gene Fusion System (Amersham Pharmacia Biotech, Freiburg, Germany). The GST-tag was cleaved by final incubation with PreScission protease. 5 μg FLIPglu was incubated in the dark for 5 min with 0, 0.1, 0.2, 0.5, 1, 2, 4, 5, 6, 8, 10, 25, 50, or 100 mM glucose or 10 mM glucose-6-phosphate (G-6-P), 10 mM mannoheptulose (MH), 10 mM 3-O-methylglucose (3-OMG) or 2 μM glibenclamide in 100 μl Krebs–Ringer solution. 5 μg FLIPglu were applied to 1 or 10 mM glucose and measured over time. Recombinant glucokinase was expressed as described earlier [35]. 5 μg FLIPglu was analyzed over time in the presence or absence of glucokinase in 100 μl HEPES buffer supplemented with ATP, $MgCl_2$ and 1, 10 or 100 mM glucose. Finally, ECFP (460 nm) and citrine (544 nm) fluorescence emission upon ECFP excitation (430 nm) were recorded in a microplate in a Labsystems Fluoroskan Ascent Counter (Thermo Fisher Scientific, Waltham, MA, USA).

2.3. Western blot

MIN6-FLIPglu, RINm5F, INS1E, COS, and mouse islets were homogenized in PBS (pH 7.4), and insoluble material was pelleted by centrifugation. Protein concentration was quantified by the Bradford protein assay. 40 μg (cells) or 35 μg (islets) protein was fractionated by reducing 10% SDS-PAGE and electroblotted onto polyvinylidene difluoride membranes. Non-specific binding sites were blocked with Odyssey Blocking Buffer (Licor Biosciences, Lincoln, NE, USA) for 1 h at room temperature. Blots were incubated with GLUT1 (~100 kDa, sc-7903, diluted 1:500, Santa Cruz Biotechnology, Santa Cruz, CA, USA), GLUT2 (~57 kDa, ab-54460, diluted 1:500, Abcam, Cambridge, U.K.), GK (~50 kDa, sc-7908, diluted 1:200, Santa Cruz Biotechnology), or HK (~120 kDa, sc-28885, diluted 1:200, Santa Cruz Biotechnology) antibody overnight at 4 °C and then with the appropriate IRDye 800CW (Licor Biosciences) secondary antibody for 30 min at room temperature. Blots were stripped with Re-blot plus (Millipore, Billerica, MA, USA) to analyze HK1 and glucokinase, or GLUT1 and GLUT2 in the same fraction. Immunoreactivity was visualized using the Licor Infrared Imaging System (Licor Biosciences).

2.4. Fluorescence microscopy

A cellR/Olympus IX81 (Olympus, Hamburg, Germany) inverted microscope system equipped with a Cellcubator (Olympus) to maintain 60% humidity, 37 °C, and 5% CO_2 was used. ECFP was excited with a D436/10 filter (AHF Analysentechnik, Tübingen, Germany). ECFP and citrine emission were detected simultaneously using a DV-CC Dual View System (Optical Insights LLC, Tucson, AZ) equipped with a 505 dcxr beam splitter and D465/30 and HQ535/30 emission filters or with 455DCLP-D480/40 and 530DCLP-D560/40 filter sets (AHF Analysentechnik). Glass coverslips were mounted in a chamber. Perifusion was performed with Krebs–Ringer solution at a flow rate of 1 ml/min using a peristaltic pump (Ismatec, Zürich, Switzerland). Images were taken every 2 s with an UPLSAPO 60×1.35 numerical aperture oil-immersion objective (Olympus). For combined analysis of Ca^{2+} and FLIPglu, MIN6-FLIPglu cells were loaded with fura-2 acetoxymethyl ester by incubation in Krebs–Ringer solution containing 25 mM HEPES for 30 min at 37 °C. HC340/26-HC387/11-BS409-HC510/84 filter sets were used for fura-2 acetoxymethyl ester, and images were obtained simultaneously every 5 s. Automated solution switching by the perifusion system entailed a lag time of 70 s until the compound concentration was reached. Recordings shown in the figures are corrected for this delay. For multiple image analysis of MIN6-FLIPglu cells on 6-well plates, an UPLSAPO 20×0.75 numerical aperture objective and scanR software (Olympus) were used. The image focus was automatically determined from transmitted light images using a gradient method. After background correction, individual cells were automatically detected using an edge detection method and tracked over time.

2.5. Measurement of glucose and pyruvate

Batches of 2×10^6 cells were incubated for 1, 2, 3, 5, 7, 9, or 10 min at 37 °C and 300 rpm in 1 ml Krebs–Ringer solution in the presence of 10 mM glucose. Batches incubated for 10 min were centrifuged, washed, and incubated for 1, 2, 3, 5, 7, or 10 min in Krebs–Ringer solution without glucose. At the end point, all samples were centrifuged and the supernatant removed. After addition of 1 ml Krebs–Ringer solution, the samples were heated for 5 min to 95 °C and finally centrifuged. Glucose was determined in the supernatant using the glucose-oxidase/peroxidase/o-dianisidin method and pyruvate by measuring the oxidation of reduced nicotinamide adenine dinucleotide in the presence of lactate dehydrogenase.

2.6. Insulin secretion

For static incubation, MIN6-FLIPglu cells were seeded in 6-well microplates at a density of 3×10^5 cells and grown for 3 days. Thereafter, cells were incubated for 1 h in bicarbonate-buffered Krebs–Ringer solution without glucose supplemented with 0.1% albumin and subsequently incubated for 1 h without glucose, with 10 mM glucose or 40 mM KCl. Thereafter, 1 ml of the incubation buffer from each well was collected

and gently centrifuged to remove detached cells. The secreted insulin was measured in the final supernatants radioimmunologically.

2.7. Statistical analysis

Statistical analyses and curve fitting were performed using the Prism analysis program (Graphpad, San Diego, CA, USA).

3. Results

3.1. Measurement of intracellular glucose using FLIPglu

Glucose concentration was evaluated by two-channel fluorescence analysis of the FLII^{12}Pglu-700μ-δ6 (FLIPglu) nanosensor. Fluorescence of citrine emission upon ECFP excitation and ECFP emission upon ECFP excitation were determined and the citrine$_{em}$/ECFP$_{em}$ upon ECFP excitation ratio calculated. For direct comparison of individual experiments, the ratio calculated at 0 mM glucose was set to 1 and values were presented as normalized ratios.

The in vitro titration of recombinant purified FLIPglu exhibited a linear range for the change in citrine$_{em}$/ECFP$_{em}$ ratio between 1 and 10 mM glucose (Fig. 1A). The binding constant for glucose was determined to be 4.223 ± 1.745 mM with a maximal normalized citrine$_{em}$/ECFP$_{em}$ ratio change of 0.43 using a single site binding equation (Citrine$_{em}$/ECFP$_{em}$ ratio = maximum specific binding∗[glucose]/(Kd + [glucose]) + slope of nonspecific binding∗[glucose] + background). The response of FLIPglu was fast and the citrine$_{em}$/ECFP$_{em}$ ratio was stable over time (Fig. 1B). Addition of G-6-P (10 mM), 3-OMG (10 mM), MH (10 mM) or glibenclamide (2 μM) in the absence of glucose did not change the citrine$_{em}$/ECFP$_{em}$ ratio, confirming that the compounds did not interact with the FLII^{12}Pglu-700μ-δ6 nanosensor (Fig. 1C). Glucokinase significantly reduced the citrine$_{em}$/ECFP$_{em}$ ratio within 1 min in the presence of ATP and 1, 10 or 100 mM glucose (Fig. 1D). Thus, the FLII^{12}Pglu-700μ-δ6 nanosensor was suitable to measure glucose phosphorylation in vitro.

MIN6 cells stably expressing FLIPglu were analyzed using a medium throughput microscopy approach with automated cell detection and calculation of the citrine$_{em}$/ECFP$_{em}$ ratio. MIN6-FLIPglu cells showed a significantly higher citrine$_{em}$/ECFP$_{em}$ ratio when incubated

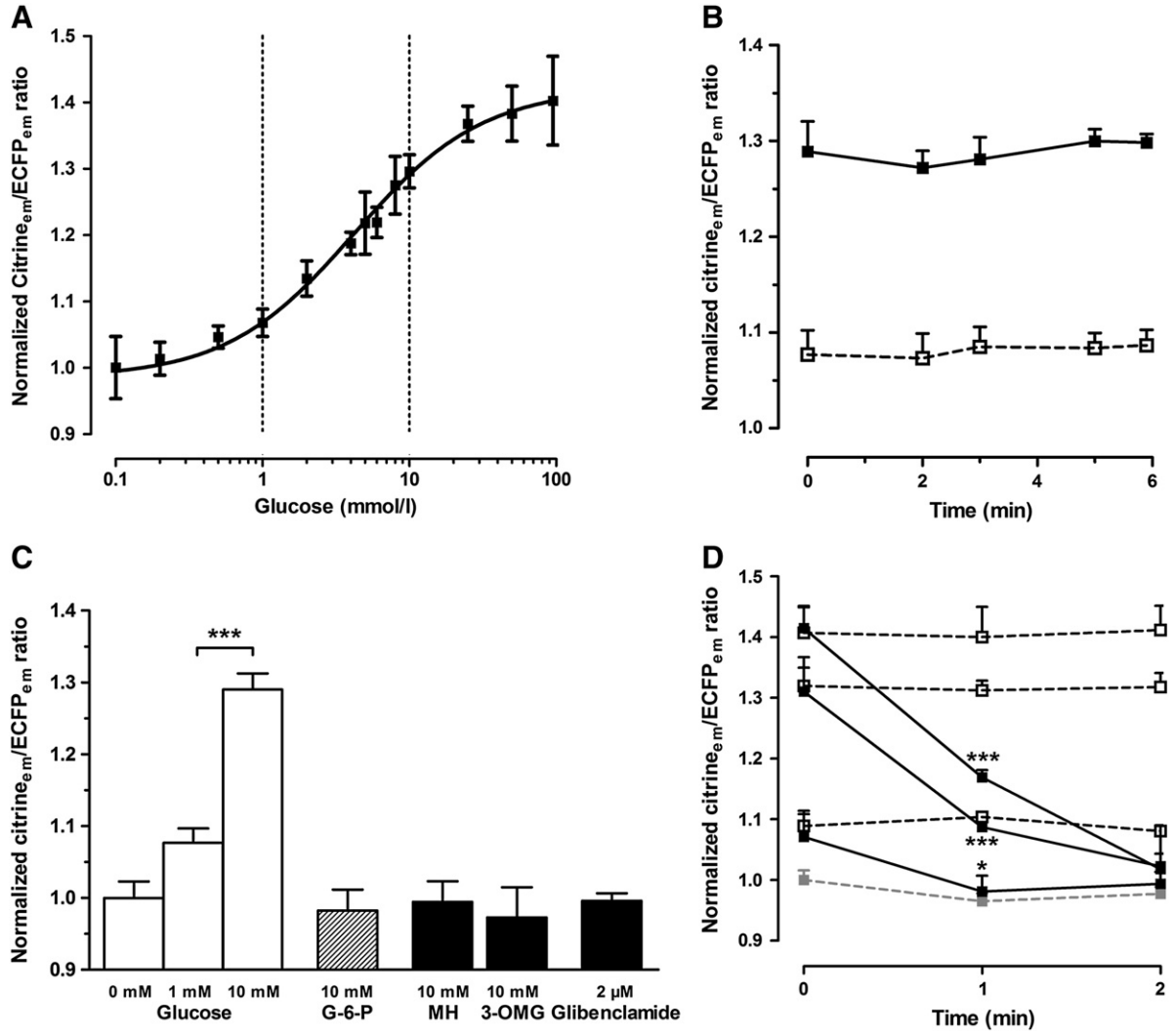

Fig. 1. Glucose analysis using the FLIPglu nanosensor. Recombinant FLIPglu was analyzed using a microplate fluorimeter. (A) FLIPglu was incubated for 5 min in the presence of different glucose concentrations. Mean normalized citrine$_{em}$/ECFP$_{em}$ ratios ± SEM of three individual experiments are shown. (B) FLIPglu was treated with 1 mM (open squares and dotted line) or 10 mM (black squares and solid line) glucose. The citrine$_{em}$/ECFP$_{em}$ ratio was measured directly or after 2, 3, 5, and 6 min. (C) FLIPglu was incubated for 5 min with glucose (0, 1, or 10 mM) or G-6-P (10 mM), MH (10 mM), 3-OMG (10 mM) or glibenclamide (2 μM). Mean normalized citrine$_{em}$/ECFP$_{em}$ ratios ± SEM of two individual experiments are shown. ***p<0.001 compared to 0 mM glucose (ANOVA/Bonferroni's multiple comparison test). (D) FLIPglu was treated without (gray squares and dotted line) or with 1 (lower line), 10 (middle line) or 100 (upper line) mM glucose in the absence (open squares and dotted line) or presence (black squares and solid line) of glucokinase. The citrine$_{em}$/ECFP$_{em}$ ratio was measured directly or after 1 and 2 min. *p<0.05; ***p<0.001 compared to the corresponding glucose concentration without glucokinase (ANOVA/Bonferroni's multiple comparison test).

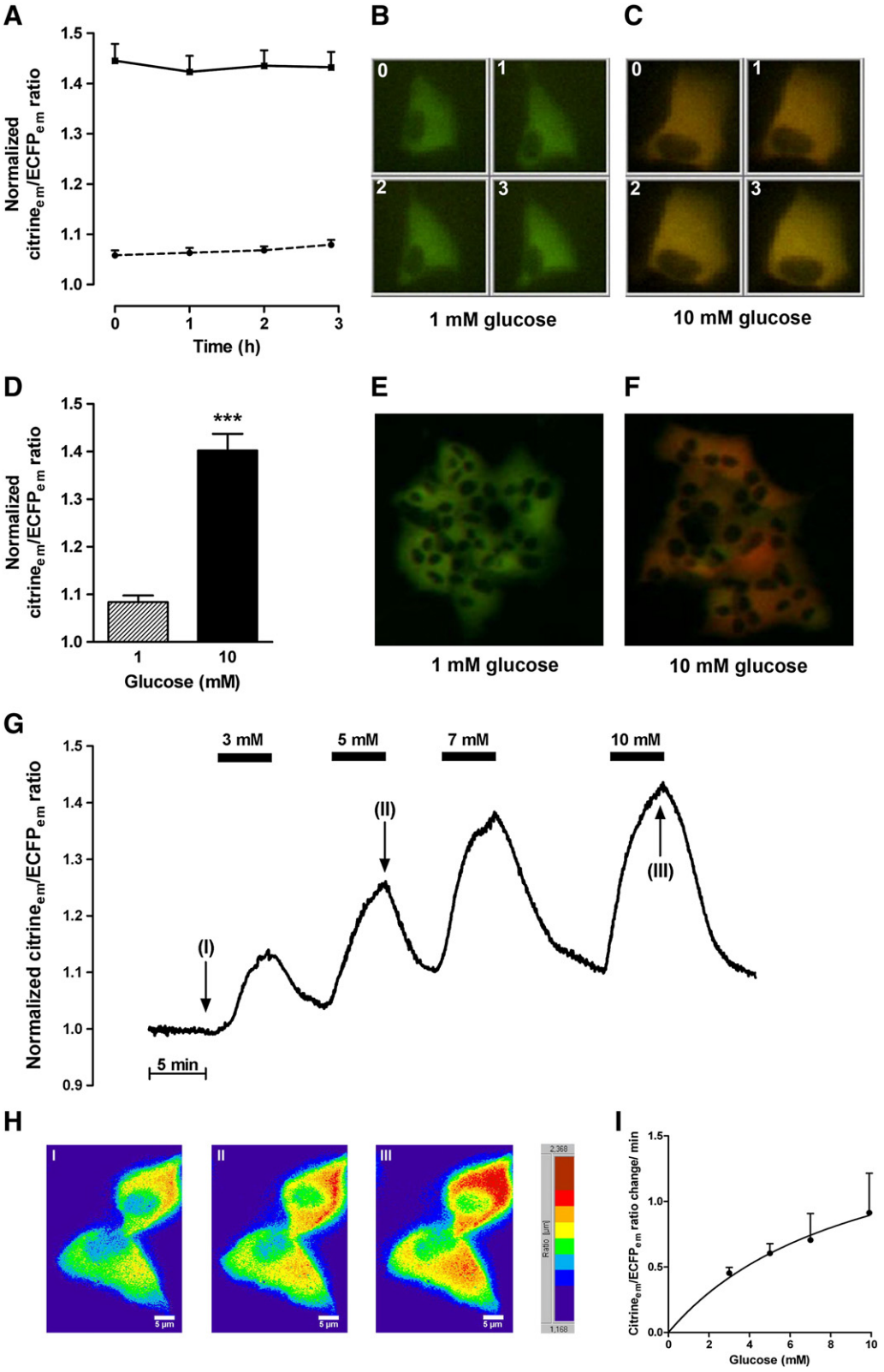

Fig. 2. Intracellular glucose concentration in MIN6 cells. MIN6-FLIPglu cells were analyzed by medium throughput microscopy. Fluorescence images were taken automatically either hourly over 4 h (A–C) or after 1 h (D–G). Images show the citrine$_{em}$/ECFP$_{em}$ ratio as a green/red merged image in a representative cell over time (B, C) or cell cluster (E, F) incubated in 1 mM (A, black circles and dotted line; B, D, striped bar; E) or 10 mM (A, black squares and solid line; C, D, black bar; F) glucose. Shown are mean values ± SEM from two individual experiments with a total of 201–235 traced cells (A) or 3753–5534 cells (D) analyzed; ***$p<0.001$ (Student's t test). MIN6-FLIPglu cells were perifused in turn without or with increasing glucose concentrations as indicated by the bars. Fluorescence images were acquired every 2 s. (G) Normalized mean ratio traces of two individual experiments analyzing a total of 8 cells are shown. (H) Pseudocolored ratio images illustrate the ratio change at the three indicated time points (I–III) in two representative cells. (I) Fitted Michaelis–Menten kinetics of glucose influx as measured from the initial citrine$_{em}$/ECFP$_{em}$ ratio change when glucose was added in the indicated concentration.

at 10 mM (1.402 ± 0.035) than at 1 mM (1.084 ± 0.014) glucose (Fig. 2A–F). The ratio change was stable over time (Fig. 2A–C) and independent from the individual cell morphology (Fig. 2D–F).

Perifusion experiments revealed, in greater detail, the correlation between the change in the citrine$_{em}$/ECFP$_{em}$ ratio and the external glucose concentration in MIN6-FLIPglu cells (Fig. 2G). Glucose increased uniformly in the cytoplasm of MIN6 cells (Fig. 2H). Glucose influx was evaluated by quantifying the first 30 s of the increase in the citrine$_{em}$/ECFP$_{em}$ ratio when external glucose was increased. Finally, the rate of cytosolic glucose accumulation was compared to that of extracellular glucose (Fig. 2I). The K_m for glucose was determined to be 9.6 mM in MIN6-FLIPglu cells.

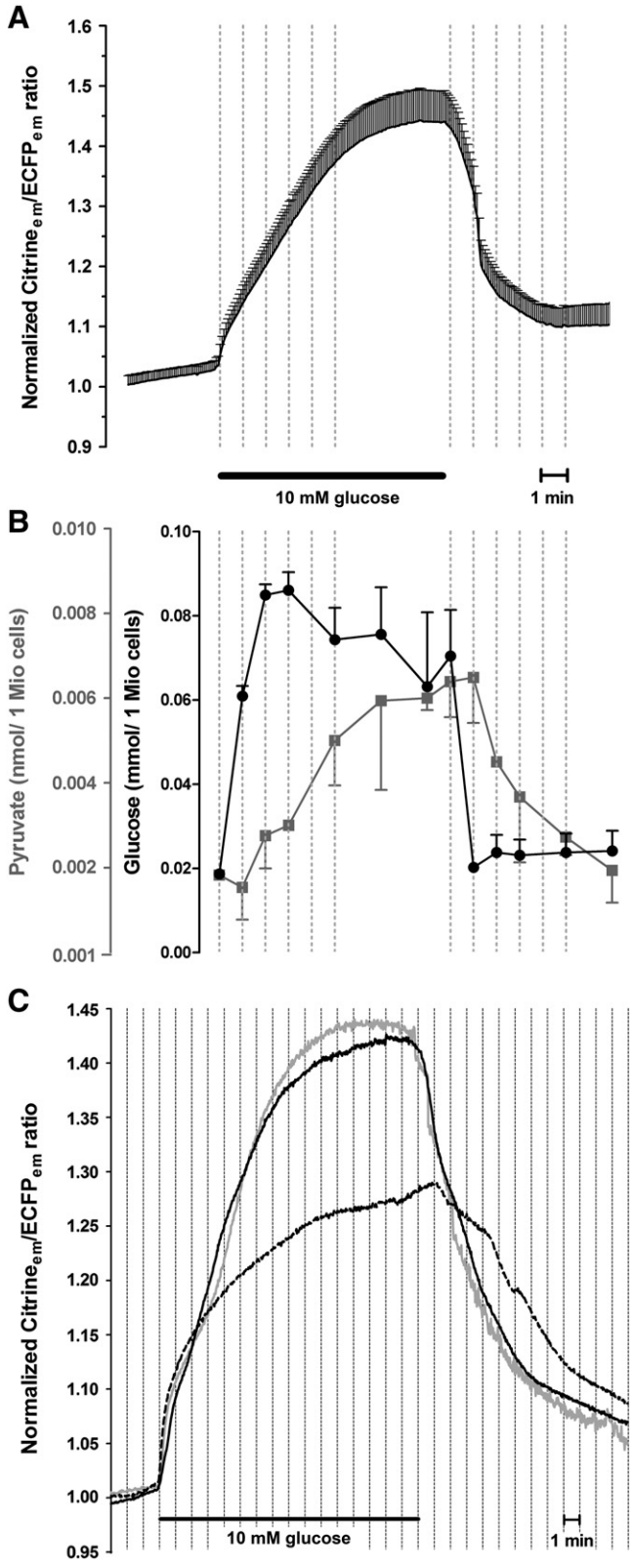

Fig. 3. Real-time intracellular glucose traces in mouse beta cells and MIN6 cells. (A) MIN6-FLIPglu cells were perifused with or without glucose (10 mM) as indicated. Fluorescence images were acquired every 2 s. A mean normalized citrine$_{em}$/ECFP$_{em}$ ratio trace ± SEM of 10 individual cells is shown. (B) Glucose (black circles) and pyruvate (gray square) content was determined in MIN6 cells by end-point measurements after incubation in Krebs–Ringer solution for 1, 2, 3, 5, 7, 9, or 10 min with 10 mM glucose or after 10 min with 10 mM glucose plus 1, 2, 3, 5, 7, or 10 min without glucose. Shown are mean values ± SEM for four individual experiments. (C) FLIPglu-expressing mouse beta cells were perifused with or without glucose (10 mM) (gray line) as indicated. In addition, glucose perifusion was performed in the presence of MH (10 mM), (dotted line) or 3-OMG (10 mM), (black line). Fluorescence images were acquired every 2 s. A mean normalized citrine$_{em}$/ECFP$_{em}$ ratio trace for 8 individual cells is shown.

3.2. Effects of 3-OMG and MH on the intracellular glucose concentration

MIN6-FLIPglu cells were perifused with or without 10 mM glucose and the intracellular glucose concentration measured every 2 s (Fig. 3A). The addition of glucose to the medium evoked a rapid initial increase of glucose in MIN6 cells. Thereafter, the increase in intracellular glucose decelerated and stabilized. Removal of glucose from the medium resulted in an immediate intracellular decrease in MIN6 cells (Fig. 3A). The glucose and pyruvate content in MIN6 cells was calculated by end-point measurements (Fig. 3B). Glucose increased over 3 min directly after external supply, and pyruvate followed with a delay of 2 min. After removal from the medium, glucose decreased rapidly within 1 min, whereas pyruvate declined slowly over 3 min in MIN6 cells (Fig. 3B).

Primary mouse beta cells exhibited an intracellular glucose concentration trace after glucose supply and removal comparable to that of MIN6 cells (Fig. 3C). Addition of 3-OMG (10 mM) in the presence of glucose (10 mM) resulted in a deceleration of the initial increase in the intracellular glucose concentration, whereas the steady state glucose concentration remained unchanged. In contrast, MH (10 mM) reduced the steady state glucose concentration. About that a slower decrease in the intracellular glucose concentration was detected after the removal of glucose from the medium (Fig. 3C).

Mouse beta cells were compared to a glucose responsive mouse and rat beta cell line, namely MIN6 and INS1E cells as well as to a passage of insulin-producing but glucose unresponsive RINm5F cells and to non-insulin-producing COS cells with respect to glucose uptake and metabolism. Glucose influx, efflux, and metabolism, as well as the intracellular glucose concentration, were calculated from the citrine$_{em}$/ECFP$_{em}$ ratio traces (Fig. 3A and C) as follows. Glucose influx was evaluated by quantifying the first 30 s of the increase in the citrine$_{em}$/ECFP$_{em}$ ratio when external glucose was increased from 0 to 10 mM (Fig. 4A). MIN6, COS, and RINm5F cells exhibited a 38%, 85%, and 85%, respectively, slower glucose influx, whereas INS1E cells showed a similar glucose influx compared to mouse beta cells. Glucose influx was diminished in mouse beta, MIN6, COS, INS1E, and RINm5F cells by 40%, 89%, 85%, 45%, and 48%, respectively, in response to 3-OMG (10 mM) (Fig. 4A). Supplementation with MH (10 mM) did not affect glucose influx. Glucose efflux and metabolism were evaluated by quantifying the first 60 s of the decrease in the citrine$_{em}$/ECFP$_{em}$ ratio when external glucose was reduced from 10 to 0 mM (Fig. 4B). Glucose efflux and metabolism were comparable in mouse beta and MIN6 cells and 11% higher in INS1E cells. In contrast, COS and RINm5F cells exhibited an 81% and 79%, respectively, slower glucose efflux and metabolism compared to mouse beta cells. The glucose efflux/metabolism rate was significantly reduced in mouse beta, MIN6, and INS1E cells in the presence of MH (10 mM), by 49%, 45%, and 55%, respectively. This reduction was not

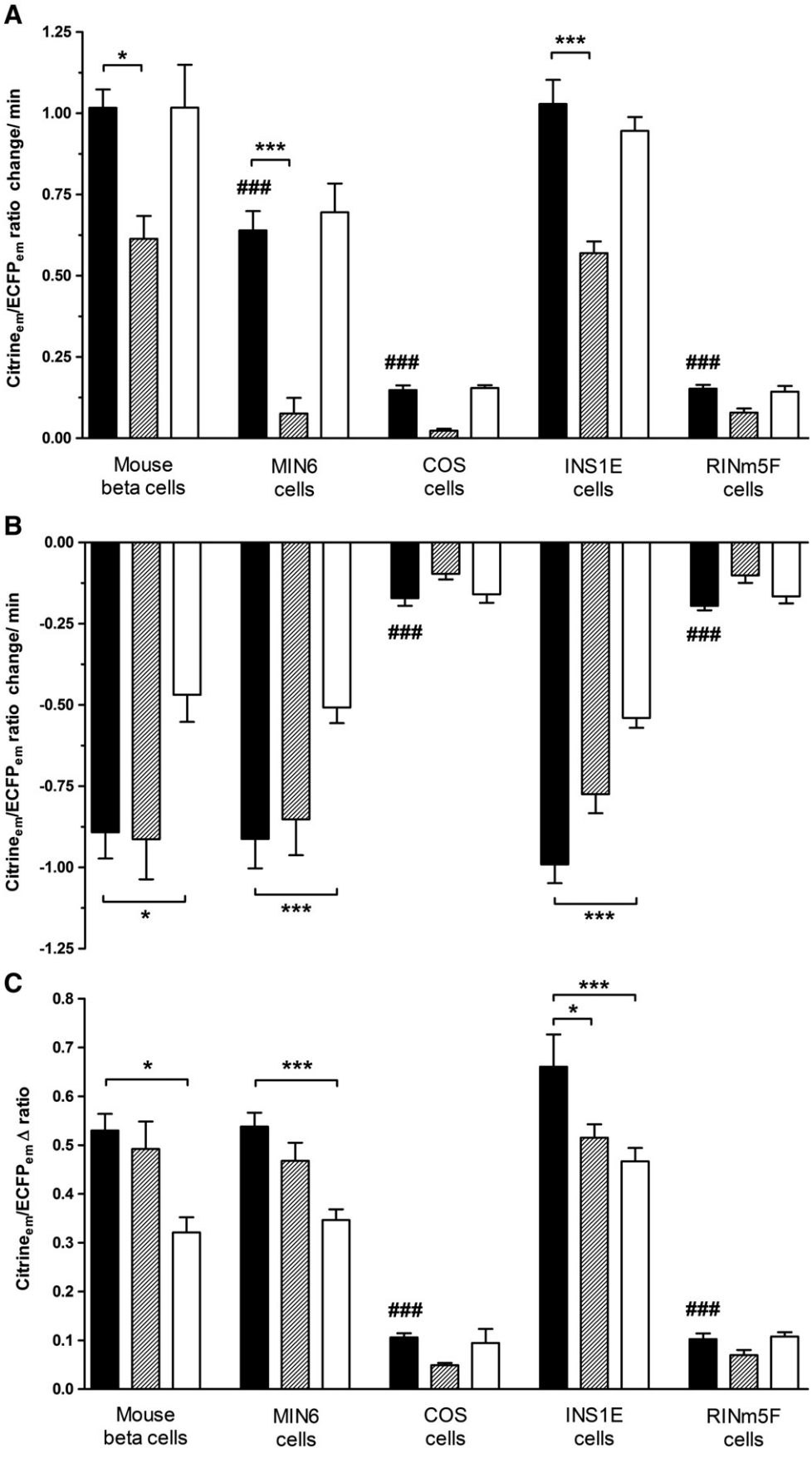
A
B
C
Citrine$_{em}$/ECFP$_{em}$ ratio change/ min
Citrine$_{em}$/ECFP$_{em}$ Δ ratio
1.25
1.00
0.75
0.50
0.25
0.00
-0.25
-0.50
-0.75
-1.00
-1.25
0.8
0.7
0.6
0.5
0.4
0.3
0.2
0.1
0.0
*
***
###
Mouse beta cells
MIN6 cells
COS cells
INS1E cells
RINm5F cells

observed in COS and RINm5F cells. Addition of 3-OMG (10 mM) evoked a 45%, 23%, and 47% decrease in the glucose efflux rate in COS, INS1E and RINm5F cells, respectively. This decrease was not observed in mouse beta and MIN6 cells. The intracellular glucose concentration at 10 mM extracellular glucose was evaluated by calculating the difference in the citrine$_{em}$/ECFP$_{em}$ ratio before and after equilibration with 10 mM glucose (Δ citrine$_{em}$/ECFP$_{em}$) (Fig. 4C). Overall, mouse beta, MIN6, and INS1E cells had significantly higher intracellular glucose concentrations than COS and RINm5F cells (Fig. 4C). Supplementation with MH (10 mM) resulted in a significant decrease in the intracellular glucose concentration in mouse beta, MIN6, and INS1E cells by 35%, 36%, and 36%, respectively, but not in COS and RINm5F cells. In contrast, 3-OMG reduced the intracellular glucose concentration in COS, RINm5F and INS1E cells by 55%, 32%, and 23%, but only by 7% and 14% in mouse beta and MIN6 cells, respectively.

Glucokinase, HK1, GLUT1, and GLUT2 are key regulators of glucose uptake and metabolism. Glucokinase was detected only in mouse islets, MIN6 and INS1E cells (Fig. 5). HK1 was highly produced in COS and RINm5F cells (Fig. 5). In mouse islets and MIN6 cells HK1 was also detectable, whereas the protein was not detectable in INS1E cells. COS and RINm5F cells were endowed with only a low GLUT1 protein expression and GLUT2 was absent (Fig. 5). MIN6 cells showed a higher protein expression of GLUT1 than of GLUT2, whereas the glucose transporters were nearly equally expressed in INS1E cells. In mouse islets the GLUT2 expression was higher than that of GLUT1.

To evaluate the observed differences in intracellular glucose concentration, the effect of 3-OMG (10 mM) and MH (10 mM) on insulin secretion was determined in MIN6-FLIPglu cells. Glucose-induced insulin secretion was significantly lowered by MH (10 mM), but not by 3-OMG (Fig. 6). KCl-induced insulin secretion in the presence of 3-OMG or MH was comparable to that of control (Fig. 6).

3.3. Concomitant analysis of glucose flux and calcium dynamics

The excitation and emission spectrum of the Ca^{2+} sensor fura-2 acetoxymethyl ester did not interfere with measurement of the citrine$_{em}$/ECFP$_{em}$ ratio of the FLIPglu glucose nanosensor. Thus, loading of MIN6-FLIPglu cells with the fura-2 acetoxymethyl ester allowed simultaneous analysis of intracellular glucose and $[Ca^{2+}]_i$ in real-time.

In a cluster of 10 MIN6-FLIPglu cells, intracellular glucose simultaneously increased after glucose supply (Fig. 7A, upper panel). An increase in $[Ca^{2+}]_i$ occurred within 1 min (Fig. 7A, I–III), when glucose reached a threshold of ~4 mM (Fig. 7B). However, synchronized high amplitude oscillations were not observed until the intracellular glucose concentration reached ~7 mM (Fig. 7B). After the removal of glucose from the medium, the intracellular glucose concentration decreased simultaneously in the cell cluster (Fig. 7A, upper panel). At glucose concentrations below ~7 mM (Fig. 7B), $[Ca^{2+}]_i$ declined. Subsequent perifusion with 40 mM KCl did not provoke changes in the citrine$_{em}$/ECFP$_{em}$ ratio of FLIPglu. $[Ca^{2+}]_i$ increased instantly when KCl was added to the medium (Fig. 7A). However, the amplitude of the oscillations was less than that of the glucose stimulus.

Addition of the K_{ATP} channel closing agent glibenclamide (2 μM) alone did not provoke noticeable changes in the intracellular glucose concentration (Fig. 8, upper panel). The mean increase in $[Ca^{2+}]_i$ in the presence of glibenclamide was higher as with 10 mM glucose (Figs. 7 and 8). However, glibenclamide induced only small amplitude

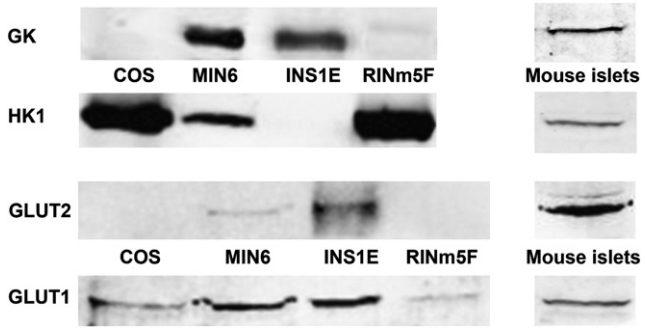

Fig. 5. Expression of glucose transporters and glucose phosphorylating enzymes. Glucokinase (~50 kDa), HK1 (~120 kDa), GLUT2 (~57 kDa), and GLUT1 (~100 kDa) expressions were analyzed in COS, MIN6, INS1E, RINm5F cells and islets by immunoblotting. Representative blots from 2 to 4 independent experiments are shown.

$[Ca^{2+}]_i$ oscillations (Fig. 8, lower panel). Addition of glucose (10 mM) to the medium resulted in an efficient increase in intracellular glucose and about that in $[Ca^{2+}]_i$ oscillations with higher amplitude (Fig. 8).

4. Discussion

The ability of beta cells to translate changes in blood glucose concentration to insulin secretion is crucial for glucose homeostasis [1–8,11]. To elucidate defects in glucose uptake, metabolism, and signal recognition under diabetic conditions, real-time glucose measurements in beta cells are of crucial importance. Measuring the extracellular glucose concentration is easy, whereas determining the intracellular glucose concentration requires sophisticated techniques [19,20,27,28]. A new fluorescence-based method to determine the intracellular glucose concentration became available through the development of FRET-based glucose sensor molecules, so-called glucose nanosensors [19,20]. The initially engineered glucose nanosensors detected the sugar in only a narrow concentration range and, therefore, were not suited for beta-cell-specific approaches [29,30]. In contrast, FLII^{12}Pglu-700μ-δ6 is a glucose nanosensor with a broad detection range at millimolar glucose concentrations [31–33]. In the present study, we applied this glucose nanosensor for the first time in primary mouse beta cells by means of adenoviral transduction.

To avoid experimental variability in the citrine$_{em}$/ECFP$_{em}$ ratio due to transfection efficiency, we generated a stable FLII^{12}Pglu-700μ-δ6-producing MIN6 cell clone. Because insulin secretion of MIN6-FLII^{12}Pglu-700μ-δ6 cells and MIN6 control cells upon glucose stimulation was comparable, interference of glucose metabolism by the nanosensor can be excluded. The citrine$_{em}$/ECFP$_{em}$ ratio observed by incubation without glucose was set to 1 in each experiment, allowing comparability between experimental groups. A similar FLII^{12}Pglu-700μ-δ6 citrine$_{em}$/ECFP$_{em}$ ratio change in response to 10 mM glucose was determined in MIN6 cells by two different approaches: static incubation in medium throughput experiments and single cell perifusion experiments. Consistent with findings in HepG2 cells by Takanaga and co-workers [32], we observed a good correlation between the in vitro glucose-binding affinity of FLII^{12}Pglu-700μ-δ6 and the in vivo normalized ratio change in MIN6 cells. In addition FLII^{12}Pglu-700μ-δ6 was able to display glucose phosphorylation by glucokinase in vitro and showed no affinity to G-6-P, confirming both adequate response and specificity of the nanosensor. Thus, estimation of the intracellular glucose concentration from the quantified citrine$_{em}$/ECFP$_{em}$ ratio [29–33]

Fig. 4. Effects of 3-OMG and MH on changes in the intracellular glucose concentration in mouse beta, MIN6, COS, INS1E and RINm5F cells. Real-time intracellular glucose traces as shown in Fig. 3 were used to calculate glucose influx, efflux, and metabolism in mouse beta, MIN6, COS, INS1E and RINm5F cells. (A) The glucose influx rate was calculated from the initial change in citrine$_{em}$/ECFP$_{em}$ ratio when the glucose concentration in the perifusion medium was changed from 0 to 10 mM glucose. (B) Glucose efflux/metabolism rate was calculated from the change in the citrine$_{em}$/ECFP$_{em}$ ratio when the glucose concentration in the perfusion medium was changed from 10 to 0 mM glucose. (C) The intracellular glucose concentration was determined as Δ citrine$_{em}$/ECFP$_{em}$ ratio before and after equilibration with 10 mM glucose. Cells were analyzed with glucose alone (10 mM) (black bars) or with 3-OMG (10 mM) (striped bars) or MH (10 mM) (open bars). Mean values ± SEM of 10–40 individual cell traces are shown. $^{*}p<0.05$; $^{***}p<0.001$ compared to controls; $^{\#\#\#}p<0.001$ compared to mouse beta cells (ANOVA/Bonferroni's multiple comparison test).

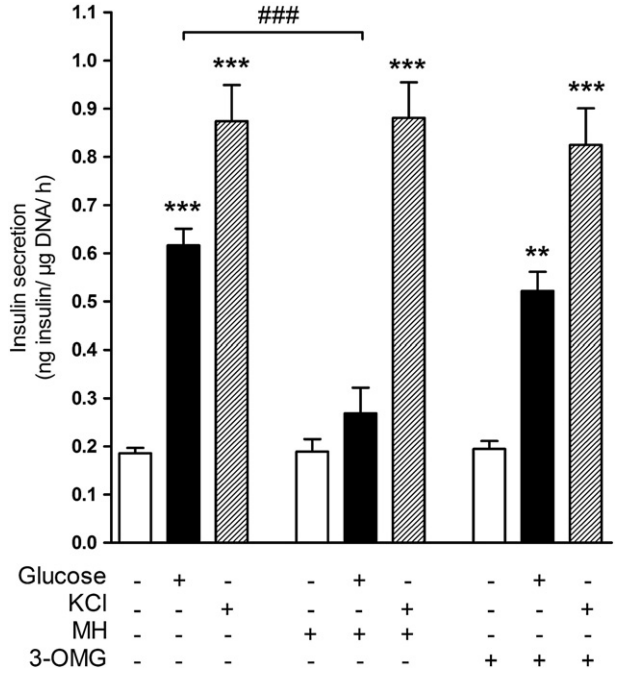

Fig. 6. Effects of MH and 3-OMG on insulin secretion in MIN6 cells. MIN6-FLIPglu cells were incubated after starvation without glucose (open bars), with glucose (10 mM) (black bars), or with KCl (40 mM) (striped bars) and MH (10 mM) or 3-OMG (10 mM). Insulin secretion is expressed per DNA content. Data are means ± SEM of four independent experiments. $^{**}p<0.01$; $^{***}p<0.001$ compared to control cells; $^{###}p<0.001$ compared to cells without compound (ANOVA/Bonferroni's multiple comparison test).

seems to be justified in cells with a high glucose turnover rate such as in beta cells.

Recent studies have suggested that a reliable estimation of the intracellular glucose accumulation rate can be achieved by calculating from the initial increase in the time-dependent ratio plots [27,32]. In our approach, the rate of glucose accumulation in the cytosol of MIN6 cells had a K_m of ~10 mM. This observation can best be explained by the mixed expression of GLUT2 and GLUT1 in MIN6 cells [1–3]. The K_m for glucose of GLUT2 has been reported to be ~17 mM, whereas GLUT1 has a very high affinity for glucose [3]. In the HepG2 hepatoma cell line, a K_m of ~1.5 for glucose was determined using the FLII^{12}Pglu-700µ-δ6 nanosensor. In agreement GLUT1 has been shown to be highly expressed in HepG2 cells, whereas GLUT2, which is mainly present in primary hepatocytes, was downregulated [32]. However, the intracellular glucose concentration is not simply determined by glucose uptake via facilitative transport, but reflects at least the sum of influx, efflux, synthesis, and metabolism.

Our results suggest that the observed plateau of the citrine$_{em}$/ECFP$_{em}$ ratio after glucose supply displays the steady state between glucose influx and metabolism in MIN6 cells. Under these conditions, glucose efflux and synthesis can be neglected in beta cells. After the initial increase in response to the glucose supply, intracellular glucose values determined by conventional end-point measurements showed high variability, whereas the high time resolution of the FLII^{12}Pglu-700µ-δ6 nanosensor kinetics revealed a further increase in intracellular glucose with decreasing slope, which finally reached a stable plateau. Intracellular glucose concentrations determined by the end-point method comprise the challenge to be contaminated with extracellular glucose and impaired by the treatment procedure. To gain further inside into the intracellular glucose metabolism we have measured the pyruvate concentration. During the slow increase of the glucose concentration, the pyruvate concentration increased, indicating accelerated glucose metabolism. The pyruvate concentration curve reached the plateau together with the FLII^{12}Pglu-700µ-δ6 nanosensor kinetics, indicating that the real-time method in fact displays the intracellular equilibration of glucose influx, efflux, and metabolism. After glucose removal, the intracellular concentration rapidly declined. This process is mediated by glucose phosphorylation and subsequent metabolism, as indicated by pyruvate production. Because GLUT proteins catalyze the facilitative transfer in a bidirectional manner [3], glucose efflux likewise contributes to the decrease in the intracellular glucose concentration.

At low concentrations, the non-metabolizable glucose analog 3-OMG is thought to delay the equilibration of glucose across the plasma membrane in beta cells without significantly affecting glucose-induced insulin secretion [26]. In agreement, we observed a retardation of glucose influx during perifusion of MIN6 cells with 10 mM glucose in the presence of 10 mM 3-OMG, and only a minor reduction in the intracellular glucose concentration and glucose-induced insulin secretion. Additional support for the explanation that the first initial increase in the citrine$_{em}$/ECFP$_{em}$ ratio reflects glucose influx was obtained by analyzing primary mouse beta cells. After glucose supply, this fast initial increase in the citrine$_{em}$/ECFP$_{em}$ ratio was detectable, but absent in the presence of 3-OMG. The slow glucose influx rate and higher responsiveness of MIN6 cells to 3-OMG compared to primary mouse beta cells can be explained by differences in the density of GLUT1 and GLUT2 in the plasma membrane [1,3,23]. MIN6 cells showed a higher protein expression of GLUT1 than of GLUT2. Accordingly, INS1E cells, which are endowed with a higher GLUT2 production, exhibited a glucose influx and responsiveness to 3-OMG comparable to primary mouse beta cells.

In non-insulin-producing COS cells as well as in a passage of glucose unresponsive RINm5F cells, the level of glucose influx, efflux, and metabolism was significantly lower compared to primary mouse beta cells, MIN6 cells and INS1E cells. This finding is consistent with the low level of GLUT1 expression and absence of GLUT2. Because 3-OMG strongly reduced intracellular glucose in COS cells and RINm5F cells, our results emphasize the rate-limiting character of glucose uptake via GLUT1 [3]. In contrast, the rate of glucose metabolism in beta cells expressing GLUT2 together with GLUT1 is controlled at the glucose phosphorylation step [3]. Glucokinase, the glucose-phosphorylating enzyme in beta cells, acts as a glucose sensor [4–7]. Accordingly, in our studies in glucokinase expressing primary mouse beta cell, MIN6 cells, and INS1E cells the competitive glucokinase inhibitor MH [24,36] significantly diminished the intracellular glucose concentration and glucose-induced insulin secretion.

Oscillations in glucose levels have been previously reported using a glucose enzyme electrode implanted into single isolated primary islets [37,38]. Therefore, glucose oscillations were proposed to be an early intrinsic trigger for the oscillatory nature of the stimulus-secretion pathway in beta cells [37,38]. Oscillations in the intracellular glucose concentration, however, have not been determined in mouse beta cells using FLII^{12}Pglu-700µ-δ6 nanosensor-based analyses. Because random fluctuations within a narrow range were observed rather than synchronized glucose oscillations, we propose downstream metabolites, such as ATP, as pacemakers of oscillations. Recent studies support a direct interplay between ATP and $[Ca^{2+}]_i$ beyond the K_{ATP} channel pathway [17,18,39].

Fig. 7. Concomitant real-time analysis of the intracellular glucose concentration and calcium dynamics in MIN6 cells. MIN6-FLIPglu cells loaded with fura-2 acetoxymethyl ester were perifused with or without glucose (10 mM) or KCl (40 mM) as indicated by the bars. Fluorescence images were acquired simultaneously every 5 s for glucose dynamics and $[Ca^{2+}]_i$. (A) An intracellular glucose trace ± SEM averaged from 10 clustered cells attaching each other (upper panel) and corresponding $[Ca^{2+}]_i$ oscillations from three representative cells (I–III) within this cluster are shown. (B) Depicted is an overlay of the intracellular glucose (black) and $[Ca^{2+}]_i$ (gray) trace ± SEM from clustered cells. Typical recordings from five independent experiments are shown.

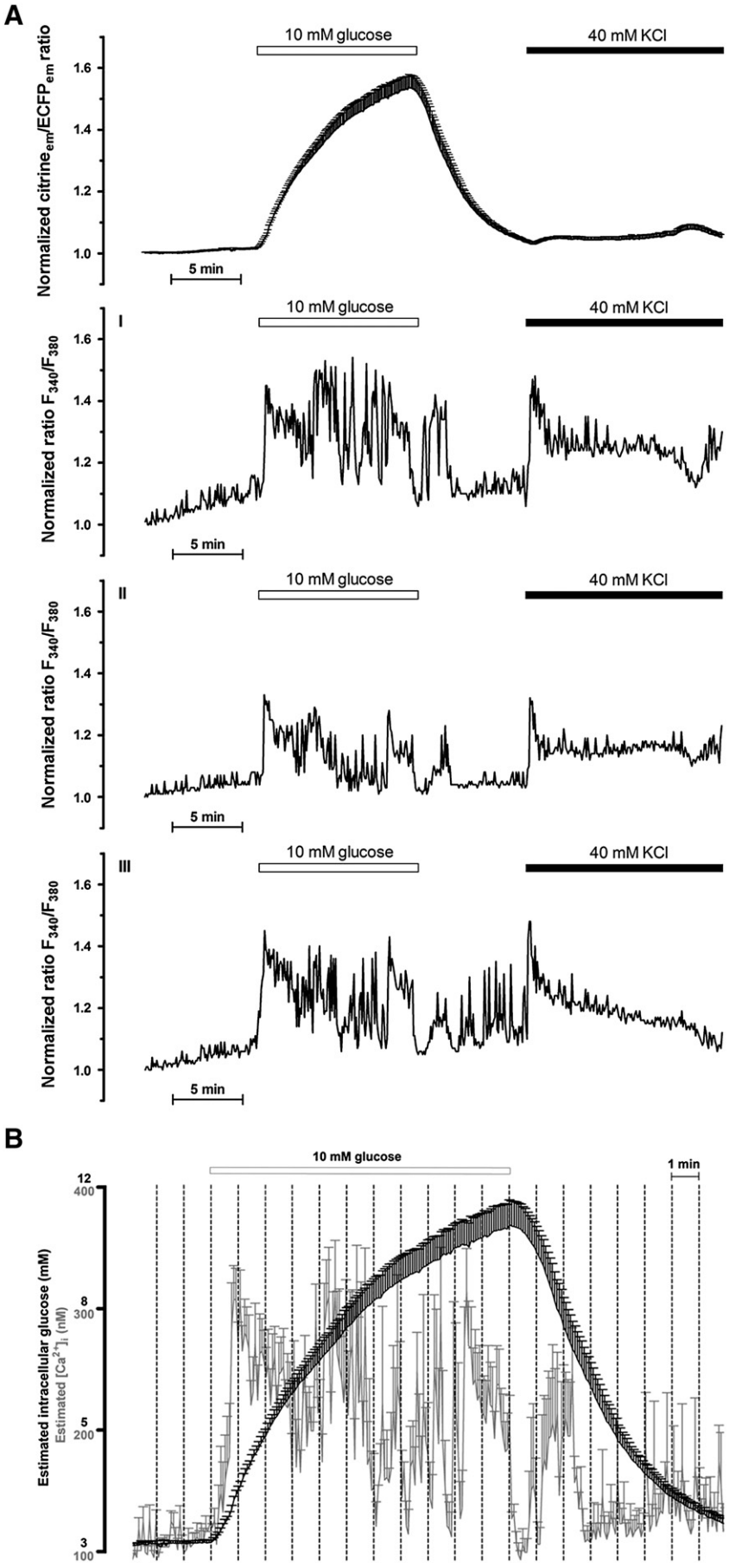
A
10 mM glucose
40 mM KCl
Normalized citrine$_{em}$/ECFP$_{em}$ ratio
1.6
1.4
1.2
1.0
5 min
I
II
III
Normalized ratio F$_{340}$/F$_{380}$
B
1 min
Estimated intracellular glucose (mM)
Estimated [Ca^{2+}]$_i$ (nM)
12
8
5
3
400
300
200
100

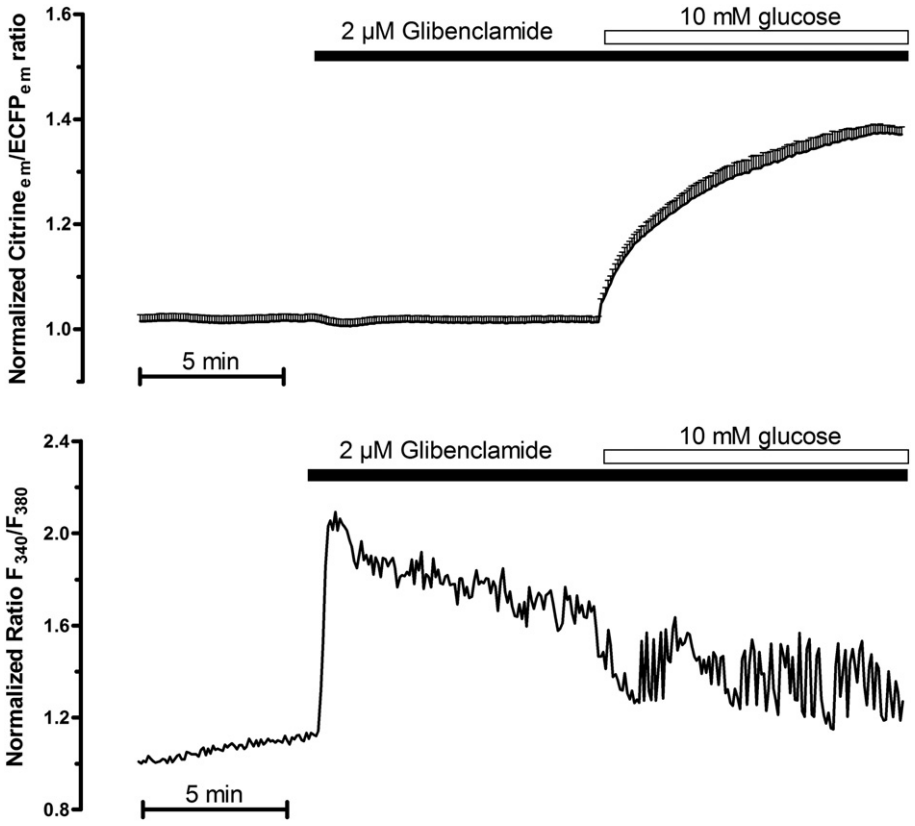

Fig. 8. Effects of glibenclamide on the intracellular glucose concentration and calcium dynamics in MIN6 cells. MIN6-FLIPglu cells loaded with fura-2 acetoxymethyl ester were perifused with glibenclamide (2 μM) in the presence or absence of glucose (10 mM) as indicated by the bars. Fluorescence images were acquired simultaneously every 5 s for glucose dynamics and $[Ca^{2+}]_i$. An intracellular glucose trace ± SEM averaged from 6 clustered cells attaching to each other (upper panel) and corresponding $[Ca^{2+}]_i$ oscillations from a representative cell within this cluster (lower panel) are shown. Typical recordings from four independent experiments are shown.

Concomitant real-time analyses of intracellular glucose and $[Ca^{2+}]_i$ have not been explored in beta cells previously. In agreement with studies in primary beta cells [8,9,15,40,41], in response to glucose, $[Ca^{2+}]_i$ showed after a short delay an initial increase with subsequent pronounced oscillations in MIN6 cells. The typical delay [8] between the increase in the extracellular glucose concentration and the $[Ca^{2+}]_i$ elevation observed in this study was somewhat shorter compared to whole pancreatic islets, most likely due to the MIN6 beta cell monolayer. We observed a threshold of ~4 mM glucose for the $[Ca^{2+}]_i$ increase. This glucose concentration is close to the inflection point of the sigmoidal activity curve of glucokinase, facilitating a fast switch to a higher rate of glucose metabolism. Thus, in the initial phase glucose uptake is balanced by metabolism, subsequently producing the ATP required for closure of the K_{ATP} channels. Not till then the intracellular glucose concentration equilibrated to the extracellular supply. Interestingly, the calculated threshold for the $[Ca^{2+}]_i$ decrease after glucose removal was ~7 mM glucose. Therefore, a higher intracellular glucose concentration than in the initial phase can be hypothesized to be necessary for retaining $[Ca^{2+}]_i$ oscillations and maintaining the second phase of insulin secretion. Taking into account that glucose, but not glibenclamide, is able to mediate large amplitude $[Ca^{2+}]_i$ oscillations, our study provides further evidence of glucose-induced amplifying signals for $[Ca^{2+}]_i$ that bypass K_{ATP} channels [8,12,41].

In conclusion, we have demonstrated that FLII^{12}Pglu-700μ-δ6 nanosensor-based intracellular glucose analysis is well suited for beta-cell-specific approaches. Concomitant real-time analysis with $[Ca^{2+}]_i$, and in future studies other key regulators, such as ATP, will provide further insight into the regulation of glucose-induced insulin secretion in pancreatic beta cells and may help to elucidate defects in diabetic conditions.

Acknowledgement

We thank Dr. W. Frommer and Dr. H. Takanaga (Stanford, CA, USA) for providing the FLII^{12}Pglu-700μ-δ6 construct (Addgene plasmid 17866), and Dr. B. Vogelstein (Baltimore, MD) for providing the vectors of the adenoviral expression system. We thank M. Funk, J. Kresse, B. Leß, and R. Waterstradt for skillful technical assistance. This work was supported by the European Commission (Integrated Project EuroDia LSHM-CT-2006-518153 in the Framework Programme 6 [FP6] and the Innovative Medicine Initiative (Joint Undertaking IMIDIA, grant agreement 115005 in the Framework Programme 7).

References

[1] F.C. Schuit, Is GLUT2 required for glucose sensing? Diabetologia 40 (1997) 104–111.
[2] B. Thorens, Molecular and cellular physiology of GLUT-2, a high-Km facilitated diffusion glucose transporter, Int. Rev. Cytol. 137 (1992) 209–238.
[3] B. Thorens, M. Mueckler, Glucose transporters in the 21st century, Am. J. Physiol. Endocrinol. Metab. 298 (2010) E141–E145.
[4] S. Baltrusch, M. Tiedge, Glucokinase regulatory network in pancreatic beta-cells and liver, Diabetes 55 (Suppl. 2) (2006) S55–S64.
[5] S. Lenzen, Glucokinase: Signal recognition enzyme for glucose-induced insulin secretion, In: in: P.R.e. Flatt (Ed.), Nutrient Regulation of Insulin Secretion, Portland Press, London and Chapel Hill, 1992, pp. 101–125.
[6] S. Lenzen, U. Panten, Signal recognition by pancreatic B-cells, Biochem. Pharmacol. 37 (1988) 371–378.
[7] F.M. Matschinsky, Banting Lecture 1995. A lesson in metabolic regulation inspired by the glucokinase glucose sensor paradigm, Diabetes 45 (1996) 223–241.
[8] J.C. Henquin, Regulation of insulin secretion: a matter of phase control and amplitude modulation, Diabetologia 52 (2009) 739–751.
[9] S. Baltrusch, S. Lenzen, Regulation of $[Ca^{2+}]_i$ oscillations in mouse pancreatic islets by adrenergic agonists, Biochem. Biophys. Res. Commun. 363 (2007) 1038–1043.
[10] S. Lenzen, M. Lerch, T. Peckmann, M. Tiedge, Differential regulation of $[Ca^{2+}]_i$ oscillations in mouse pancreatic islets by glucose, alpha-ketoisocaproic acid,

glyceraldehyde and glycolytic intermediates, Biochim. Biophys. Acta 1523 (2000) 65–72.
[11] P. Rorsman, E. Renstrom, Insulin granule dynamics in pancreatic beta cells, Diabetologia 46 (2003) 1029–1045.
[12] J.C. Henquin, Triggering and amplifying pathways of regulation of insulin secretion by glucose, Diabetes 49 (2000) 1751–1760.
[13] A. Miyawaki, J. Llopis, R. Heim, J.M. McCaffery, J.A. Adams, M. Ikura, R.Y. Tsien, Fluorescent indicators for Ca^{2+} based on green fluorescent proteins and calmodulin, Nature 388 (1997) 882–887.
[14] S.R. Adams, A.T. Harootunian, Y.J. Buechler, S.S. Taylor, R.Y. Tsien, Fluorescence ratio imaging of cyclic AMP in single cells, Nature 349 (1991) 694–697.
[15] O. Dyachok, Y. Isakov, J. Sagetorp, A. Tengholm, Oscillations of cyclic AMP in hormone-stimulated insulin-secreting beta-cells, Nature 439 (2006) 349–352.
[16] J. Berg, Y.P. Hung, G. Yellen, A genetically encoded fluorescent reporter of ATP: ADP ratio, Nat. Methods 6 (2009) 161–166.
[17] E. Heart, R.F. Corkey, J.D. Wikstrom, O.S. Shirihai, B.E. Corkey, Glucose-dependent increase in mitochondrial membrane potential, but not cytoplasmic calcium, correlates with insulin secretion in single islet cells, Am. J. Physiol. Endocrinol. Metab. 290 (2006) E143–E148.
[18] H.J. Kennedy, A.E. Pouli, E.K. Ainscow, L.S. Jouaville, R. Rizzuto, G.A. Rutter, Glucose generates sub-plasma membrane ATP microdomains in single islet beta-cells. Potential role for strategically located mitochondria, J. Biol. Chem. 274 (1999) 13281–13291.
[19] M. Fehr, S. Okumoto, K. Deuschle, I. Lager, L.L. Looger, J. Persson, L. Kozhukh, S. Lalonde, W.B. Frommer, Development and use of fluorescent nanosensors for metabolite imaging in living cells, Biochem. Soc. Trans. 33 (2005) 287–290.
[20] S. Lalonde, D.W. Ehrhardt, W.B. Frommer, Shining light on signaling and metabolic networks by genetically encoded biosensors, Curr. Opin. Plant Biol. 8 (2005) 574–581.
[21] M. Tiedge, S. Baltrusch, New perspectives of imaging techniques in islet research, Dtsch. Med. Wochenschr. 136 (2011) 1130–1134.
[22] S. Baltrusch, S. Langer, L. Massa, M. Tiedge, S. Lenzen, Improved metabolic stimulus for glucose-induced insulin secretion through GK and PFK-2/FBPase-2 coexpression in insulin-producing RINm5F cells, Endocrinology 147 (2006) 5768–5776.
[23] H. Heimberg, A. De Vos, D. Pipeleers, B. Thorens, F. Schuit, Differences in glucose transporter gene expression between rat pancreatic alpha- and beta-cells are correlated to differences in glucose transport but not in glucose utilization, J. Biol. Chem. 270 (1995) 8971–8975.
[24] J. Rasschaert, M.M. Kadiata, W.J. Malaisse, Effects of D-mannoheptulose upon D-glucose metabolism in tumoral pancreatic islet cells, Mol. Cell. Biochem. 226 (2001) 77–81.
[25] A. Sener, F. Malaisse-Lagae, W.J. Malaisse, Hexose metabolism in pancreatic islets: time-course of the oxidative response to D-glucose, Biochim. Biophys. Acta 1177 (1993) 54–60.
[26] A. Sener, O. Scruel, K. Louchami, H. Jijakli, W.J. Malaisse, Inhibition of glucose-induced insulin release by 3-O-methyl-D-glucose: enzymatic, metabolic and cationic determinants, Mol. Cell. Biochem. 194 (1999) 133–145.
[27] K. Yamada, M. Nakata, N. Horimoto, M. Saito, H. Matsuoka, N. Inagaki, Measurement of glucose uptake and intracellular calcium concentration in single, living pancreatic beta-cells, J. Biol. Chem. 275 (2000) 22278–22283.
[28] K. Yamada, M. Saito, H. Matsuoka, N. Inagaki, A real-time method of imaging glucose uptake in single, living mammalian cells, Nat. Protoc. 2 (2007) 753–762.
[29] M. Fehr, S. Lalonde, D.W. Ehrhardt, W.B. Frommer, Live imaging of glucose homeostasis in nuclei of COS-7 cells, J. Fluoresc. 14 (2004) 603–609.
[30] M. Fehr, S. Lalonde, I. Lager, M.W. Wolff, W.B. Frommer, In vivo imaging of the dynamics of glucose uptake in the cytosol of COS-7 cells by fluorescent nanosensors, J. Biol. Chem. 278 (2003) 19127–19133.
[31] B.H. Hou, H. Takanaga, O. Griesbeck, W.B. Frommer, Osmotic induction of calcium accumulation in human embryonic kidney cells detected with a high sensitivity FRET calcium sensor, Cell Calcium 46 (2009) 130–135.
[32] H. Takanaga, B. Chaudhuri, W.B. Frommer, GLUT1 and GLUT9 as major contributors to glucose influx in HepG2 cells identified by a high sensitivity intramolecular FRET glucose sensor, Biochim. Biophys. Acta 1778 (2008) 1091–1099.
[33] H. Takanaga, W.B. Frommer, Facilitative plasma membrane transporters function during ER transit, FASEB J. 24 (2010) 2849–2858.
[34] T.C. He, S. Zhou, L.T. da Costa, J. Yu, K.W. Kinzler, B. Vogelstein, A simplified system for generating recombinant adenoviruses, Proc. Natl. Acad. Sci. U. S. A. 95 (1998) 2509–2514.
[35] S. Baltrusch, F. Francini, S. Lenzen, M. Tiedge, Interaction of glucokinase with the liver regulatory protein is conferred by leucine–asparagine motifs of the enzyme, Diabetes 54 (2005) 2829–2837.
[36] M. Tiedge, U. Krug, S. Lenzen, Modulation of human glucokinase intrinsic activity by SH reagents mirrors post-translational regulation of enzyme activity, Biochim. Biophys. Acta 1337 (1997) 175–190.
[37] S.K. Jung, L.M. Kauri, W.J. Qian, R.T. Kennedy, Correlated oscillations in glucose consumption, oxygen consumption, and intracellular free Ca(2+) in single islets of Langerhans, J. Biol. Chem. 275 (2000) 6642–6650.
[38] R.T. Kennedy, L.M. Kauri, G.M. Dahlgren, S.K. Jung, Metabolic oscillations in beta-cells, Diabetes 51 (Suppl. 1) (2002) S152–S161.
[39] P. Detimary, P. Gilon, J.C. Henquin, Interplay between cytoplasmic Ca^{2+} and the ATP/ADP ratio: a feedback control mechanism in mouse pancreatic islets, Biochem. J. 333 (1998) 269–274.
[40] O. Dyachok, O. Idevall-Hagren, J. Sagetorp, G. Tian, A. Wuttke, C. Arrieumerlou, G. Akusjarvi, E. Gylfe, A. Tengholm, Glucose-induced cyclic AMP oscillations regulate pulsatile insulin secretion, Cell Metab. 8 (2008) 26–37.
[41] S. Lenzen, T. Peckmann, Effects of tolbutamide and N-benzoyl-D-phenylalanine (NBDP) on the regulation of $[Ca^{2+}]_i$ oscillations in mouse pancreatic islets, Biochem. Pharmacol. 62 (2001) 923–928.